www.sciencemag.org/cgi/content/full/1175870/DC1

Supporting Online Material for

Bcl6 and Blimp-1 Are Reciprocal and Antagonistic Regulators of T Follicular Helper Cell Differentiation

Robert J. Johnston, Amanda C. Poholek, Daniel DiToro, Isharat Yusuf, Danelle Eto, Burton Barnett, Alexander L. Dent, Joe Craft, Shane Crotty*

*To whom correspondence should be addressed. E-mail: shane@liai.org

Published 16 July 2009 on *Science* Express
DOI: 10.1126/science.1175870

This PDF file includes:

Supplementary Materials

Methods

Mice. C57BL/6J (B6), ICOS-deficient (*Icos*$^{-/-}$, B6.129S1-*Icos*^{tm1Flv}/J) (*5*), Blimp-1 conditional knockout (*Prdm1*$^{flox/flox}$), and B6 μMT mice were purchased from the Jackson Laboratory. SAP^{-} (*Sh2d1a*$^{-}$) (*1*), OT-II CD45.1^{+}, and SMtg CD45.1^{+} (SMtg = SMARTA. LCMV gp66-77 I-A^{b} specific) (*2*) mice were all fully backcrossed to B6 (determined > 99% pure by pan-genome microsatellite analysis at LIAI) and bred at LIAI. HEL BCR-transgenic mice (MD4) were bred on a μMT background (*3*). OT-II Thy1.1 and Thy1.2 were bred at the Yale School of Medicine. B1-8 mice (NP-specific B cells) were provided by M. Shlomchik, originally from K. Rajewsky (*4*). Bcl6-deficient animals (*6*) were bred to OT-II at the Yale School of Medicine. All animal experiments were conducted in accordance with approved animal protocols.

Retroviral vectors, transductions, and cell transfers. Bcl6 and Blimp-1 cDNAs were obtained from Open Biosystems (Bcl6 Clone ID: 6309948. Prdm1 Clone ID: 40048956), sequenced in full, and complete open reading frames were cloned into the retroviral expression vector pMIG-GFP. The Blimp-1 expression construct included the natural Kozak sequence upstream of the Blimp-1 open reading frame. For *prdm1*$^{fl/fl}$ experiments, CD4^{+} T cells were co-transduced with SMARTA TCR-RV (constructed using the 2A peptide linked design of Vignali (*9*)) and with Cre-RV (constructed using the NLS-Cre sequence of Rajewsky and colleagues (*10*)). Deletion of *Prdm1* by Cre-RV was confirmed to be greater than 98% efficient by genomic DNA qPCR. Signals from primers targeting the final exon of *Prdm1* (GCTATGACTTTGGTGCTTGGGC and GACTGGATGGTGTGGTGTTTCTATC) were normalized to β-actin (*Actb*) (AGGCCAACCGTGAAAAG and GCGTGAGGGAGAGCATAG).

Virions were produced using the Plat-E cell line (*7*) as described (*8*). Naive CD4^{+} T cells were purified from whole splenocytes by negative selection using magnetic beads (Miltenyi) and suspended in D-10 (DMEM + 10% fetal calf serum (FCS), supplemented with 2mM GlutaMAX (Gibco), and 100 U/mL Penicillin/Streptomycin (Gibco)) + 10 ng/mL hIL-2. 2 x 10^{6} cells/well were stimulated in 24-well plates pre-coated with 0.5 mL anti-hamster IgG (Vector Laboratories) followed by anti-CD3 (clone 17A2, eBiosciences) and anti-CD28 (clone 37.51, eBiosciences), or directly coated with 0.5 mL of 8 μg/ml anti-CD3 and anti-CD28 (BioXcell). At 24 and 36 hours, cells were transduced as described (*8*), except centrifugations were at 30-34 °C. After a total of 72 hours of stimulation, the CD4^{+} T cells were transferred into new wells in fresh D-10 + 10 ng/mL IL-2 for an additional 72 hours, and were split as needed. When used, control untransduced cells were subjected to the same *in vitro* stimulation and culture conditions as were used for transduced cells. Transduced cells were then purified by sorting 7AAD^{-} GFP^{+} (and GFP^{-} as needed) cells on a FACSDiva or FACSAria (BD Biosciences).

Cell transfers into host mice were performed by intravenous injection via the retro-orbital sinus. Transferred cells were rested in host mice for 3-5 days before infection or immunization (*11*). For naïve SMtg CD4^{+} T cell transfers, 6,000 cells were transferred per mouse. For transduced SMtg CD4^{+} T cell transfers, 25 x 10^{3} cells were transferred. In the case of mixed experiments, 25 x 10^{3} non-transduced SMtg (GFP^{-}) and 25 x 10^{3} RV^{+} SMtg cells were transferred into a common host (50 x 10^{3} SMtg cells/mouse). For transduced OT-II CD4^{+} T cell transfers, 250 x 10^{3} cells were transferred per mouse. For experiments assessing *Bcl6*$^{-/-}$ CD4^{+} T cells, whole splenocytes containing 0.5 - 1 x 10^{6} CD4^{+} T cells and, when specified, whole splenocytes containing 1 x 10^{6} NP-specific B cells were transferred per mouse.

Infections and Immunizations. LCMV stocks were prepared and quantified as described (*8*). All infections were done by intraperitoneal injection of 1-2 x 10^{5} plaque-forming units of LCMV Armstrong per mouse. NP-Ova in alum was prepared by mixing NP(19)-Ova (Biosearch Technologies) in PBS with Alum (Pierce) at a 3:1 ratio for 60 minutes at 4 °C. NP-Ova/Alum immunizations were done by

intraperitoneal injection of 100 μg. Ova in alum was prepared and injected in a comparable manner. Splenocytes and serum were analyzed 8 days after infection or immunization, unless stated otherwise.

Bone marrow chimeras. Thy1.2 or Thy1.1 B6 recipient mice were irradiated with the equivalent of 1000 cGy (XRAD 320 Biological Irradiator, Precision X-ray, Inc.). Bone marrow from OT-II *Bcl6*$^{+/+}$ or OT-II *Bcl6*$^{-/-}$ mice was isolated with PBS and a syringe. Bone marrow cells were subjected to red cell lysis and magnetic separation to remove T cells. Approximately 1 x 10^7 cells were transferred into congenically mismatched recipients immediately after irradiation. Eight weeks later, mice were bled to confirm hematopoietic reconstitution. Splenocytes from fully reconstituted bone marrow chimeras were subsequently transferred into new sets of congenically mismatched hosts as above, followed by immunization with Ova or NP-Ova in alum.

Flow Cytometry. Single-cell suspensions of spleen were prepared by standard gentle mechanical disruption. Surface staining for flow cytometry used monoclonal antibodies to SLAM (CD150, Biolegend); CD4, PD-1, CD200, ICOS, BTLA, CD62L, B220, CD45.1/2, and Fas (BD Biosciences); CD44, TCRβ and B220 (eBiosciences), as well as Biotin/FITC-labelled peanut agglutinin (PNA) and GL7 (Vector Laboratories and BD Pharmingen, respectively). CD43 staining was done with the 1B11 clone (*12*).

For most figures, CXCR5 staining was done using purified anti-CXCR5 (BD Pharmingen) for 1 hour, followed by biotinylated anti-rat IgG (Jackson Immunoresearch), and then APC-labelled streptavidin (Caltag Laboratories) in PBS + 0.5% BSA + 2% FCS + 2% Normal Mouse Serum on ice; and samples were then acquired without fixation. For Figure 3D *Bcl6*$^{-/-}$ experiments, T_{FH} staining was done using biotinylated anti-CXCR5 for 30 minutes at room temperature, followed by PE-Cy7-conjugated streptavidin (BD Biosciences) at 4 °C.

Intracellular cytokine staining (ICS) was done in most cases with a 5 hour peptide (2.0 μg/mL) stimulation (*8*). For ICS with PMA and ionomycin stimulation, splenocytes were cultured with 20 ng/mL PMA and 1μM Ionomycin for 4 hours. Directly conjugated antibodies against IFN-γ and IL-2 (BD Pharmingen) were used. Intracellular IL-21 detection was done using an IL-21R-Fc chimeric protein (R&D Systems) followed by PE or APC-labelled anti-human IgG (Jackson Immunoresearch)(*13*).

MHC Class II tetramer was produced by oligomerizing biotinylated I-A^b-gp66 (DIYKGVYQFKSV (*14*)) monomer (NIH tetramer core) with APC-labelled streptavidin (Molecular Probes) following NIH tetramer core facility recommendations. To stain, gp66 I-A^b tetramer was incubated with splenocytes for 3 hours at 37 °C. Tetramer stained cells were washed twice and then stained on ice for additional markers prior to acquisition. Splenocytes intended for tetramer staining were obtained 10 days after LCMV infection.

Microscopy. For Figure S2, standard immunofluorescence histology was performed, as described previously (*8*), using a deconvolution confocal microscope (Marianas). For Figure 3G and S8, spleens were harvested and immediately frozen in OCT tissue-freezing medium. Sections were cut to 6μm thickness on a cryostat and stained for immunofluoresence using CD4-Pacific Blue or CD4-Alexa647 (eBioscience and BD Biosciences, respectively), biotinylated PNA (Vector Labs), IgD-FITC (BD Biosciences), and Streptavidin-Alexa555 (Invitrogen). 25x images were acquired on a Zeiss LSM 510 Meta Confocal. 10x images were acquired with an Olympus BX40 equipped with 100W mercury lamp (Olympus) and a SPOT RT CCD camera (Diagnostic Instruments) using fluorescence filters optimized for DAPI, FITC, Cy3, and Cy5 (Chroma). Images were acquired, processed to reduce background, pseudo-colored, and merged with Adobe Photoshop.

RNA, gene expression microarrays, and qPCR. Splenocytes were isolated and antigen-specific $CD4^+$ T cells were enriched using anti-CD45.1-FITC and anti-FITC magnetic bead purification (Miltenyi). T_{FH} and non-T_{FH} $CD4^+$ $CD45.1^+$ $TCR\beta^+$ $CD19^-$ $7AAD^-$ cells were then sorted on the basis of CXCR5 expression using a FACSAria (BD Biosciences). Approximately 1 x 10^6 cells from each condition (in

duplicate) were sorted directly into RNALater (Ambion). Naive SMtg $CD4^+$ T cells were obtained from intact SMtg mice, sorting for $CD4^+$ $CD45.1^+$ $CD44^{low}$ $CD62L^{high}$ $7AAD^-$. RNA was isolated using Qiagen RNAeasy Mini spin columns (Qiagen), including QiaShredder and on-column digestion of genomic DNA. Some RNA samples were then concentrated using MinElute spin columns (Qiagen). RNA quality of all samples was confirmed by BioAnalyzer Nano gel (Agilent), then probes were generated by single round linear amplification of 30 ng RNA using the Ovation Pico system (Nugen) and used on Affymetrix 430 2.0 chips. Data was analyzed using Genespring 7 (Agilent) and signals were GC-RMA preprocessed. Gene normalized signals were used for optimal analysis (median signal = 1), and gene probes without a signal of > 0.5 normalized value in at least one of three conditions (Naive, non-T_{FH}, T_{FH}) were excluded from scatter plots. Raw microarray signal data has been deposited at NCBI GEO. cDNA synthesis was performed using SuperScript II Reverse Transcriptase (Invitrogen) with oligo dT and random hexamer primed reactions that were then pooled. qPCR reactions were performed in triplicate using iTaq Sybr Green with Rox (BioRad) on a Roche Lightcycler 480, using primers described in Table 1.

Immunoblot. Bcl6 protein was detected by Western blot. Whole cell lysates were prepared using RIPA lysis buffer. Blots were probed with polyclonal anti-Bcl6 (#19, Santa Cruz Biosciences).

ELISAs. Anti-NP-Ova IgG was quantified by ELISA using NP(19)-Ova (Biosearch Technologies) as the capture antigen on 96-well Maxisorp microtiter plates (Nunc). Following incubation of sample serum or media, HRPO-conjugated goat anti-mouse IgG-γ (Caltag Laboratories) was used, or isotype specific secondary antibodies (anti-IgM, IgG1, IgG2a/c, IgG2b, IgG3. Caltag Laboratories).

Transwell Chemotaxis assay. All migration assays were performed in 24-well Transwell plates with a polycarbonate filter pore size of 5 μm (Corning Costar). $CD4^+$ T cells were purified from B6 host mice 8 days after SMtg transfer and LCMV infection. Cells were rested for 60 min in migration medium (DMEM + 2% FCS) at 37 °C in 5% CO_2 prior the start of the assay. Recombinant mouse BLC/CXCL13 (R&D Systems) was serially diluted in migration medium and added to each of the lower wells while 1 x 10^6 $CD4^+$ T cells were added to the top chambers. Cells were allowed to migrate for 90 min at 37 °C in 5% CO_2. Migrated cells from each well were collected and cell counts performed using the Accuri C6 (Accuri Cytometers). Surface staining with anti-CD4, CD45.1, CD44, and SLAM antibodies was done to phenotype an aliquot of migrants by flow cytometry. Migration was calculated for SMtg T_{FH} ($CD4^+$ $CD45.1^+$ $CD44^{high}$ $SLAM^{low}$) and non-T_{FH} ($CD4^+$ $CD45.1^+$ $CD44^{high}$ $SLAM^{high}$) as the percentage of input cells that migrated at each chemokine concentration.

Statistical Analysis. Statistical tests were performed using Prism 5.0 (GraphPad). P-values were calculated using two-tailed unpaired Student's t tests with a 95% confidence interval. Error bars depict the standard error of the mean (SEM). For experiments in which GFP^+ and GFP^- SMtg cells were co-transferred into host mice and compared, paired Student's t tests were used.

Supplementary References

1. M. J. Czar *et al.*, *Proc Natl Acad Sci U S A* **98**, 7449 (Jun 19, 2001).
2. A. Oxenius, M. F. Bachmann, R. M. Zinkernagel, H. Hengartner, *Eur. J. Immunol.* **28**, 390 (Jan 1, 1998).
3. K. B. McClellan, S. Gangappa, S. H. Speck, H. W. Virgin, *PLoS Pathog* **2**, e58 (Jun, 2006).
4. E. Sonoda *et al.*, *Immunity* **6**, 225 (Mar 1, 1997).
5. A. Tafuri *et al.*, *Nature* **409**, 105 (Jan 4, 2001).
6. A. L. Dent, A. L. Shaffer, X. Yu, D. Allman, L. M. Staudt, *Science* **276**, 589 (Apr 25, 1997).
7. S. Morita, T. Kojima, T. Kitamura, *Gene Ther* **7**, 1063 (Jun 1, 2000).
8. M. M. McCausland *et al.*, *J Immunol* **178**, 817 (Jan 15, 2007).

9. J. Holst *et al.*, *Nat Protoc* **1**, 406 (Jan 1, 2006).
10. H. Gu, Y. R. Zou, K. Rajewsky, *Cell* **73**, 1155 (Jun 18, 1993).
11. K. K. McKinstry *et al.*, *J Exp Med* **204**, 2199 (Sep 3, 2007).
12. L. E. Harrington, M. Galvan, L. G. Baum, J. D. Altman, R. Ahmed, *J Exp Med* **191**, 1241 (Apr 3, 2000).
13. A. Suto *et al.*, *J Exp Med* **205**, 1369 (Jun 9, 2008).
14. D. Homann *et al.*, *Virology* **363**, 113 (Jun 20, 2007).
15. C. S. Ma, K. E. Nichols, S. Tangye, *Annu Rev Immunol* **25**, 337 (Jan 1, 2007).
16. A. G. Castro *et al.*, *J Immunol* **163**, 5860 (Dec 1, 1999).
17. R. I. Nurieva *et al.*, *Immunity* **29**, 138 (Jul 1, 2008).
18. K. M. Ansel, L. J. McHeyzer-Williams, V. N. Ngo, M. G. McHeyzer-Williams, J. G. Cyster, *J Exp Med* **190**, 1123 (Oct 18, 1999).
19. J. K. Whitmire, M. S. Asano, K. Murali-Krishna, M. Suresh, R. Ahmed, *Journal of Virology* **72**, 8281 (Oct 1, 1998).
20. D. G. Brooks, L. Teyton, M. B. Oldstone, D. B. McGavern, *J Virol* **79**, 10514 (Aug, 2005).

Table 1. Quantitative PCR (qPCR) Primers.

Gene	Forward Primer Sequence	Reverse Primer Sequence
Bcl6	CCTGTGAAATCTGTGGCACTCG	CGCAGTTGGCTTTTGTGACG
Blimp-1	ACATAGTGAACGACCACCCCTG	CTTACCACGCCAATAACCTCTTTG
IL-21	GCTCCACAAGATGTAAAGGGGC	CCACGAGGTCAATGATGAATGTC
CXCR5	GACCTTCAACCGTGCCTTTCTC	GAACTTGCCCTCAGTCTGTAATCC
SLAM	AAAAGTGTCCGCATCCTCGTC	ATTGAAAGTGGTAGCCATCCTCC
PD-1	GCTCACTTCAGGTTTACCACAAGC	GCCCAACAGTAGGATTCAGGAGAC
ICOS	CAGGAGAAATCAATGGCTCGG	TTGGTCTTGGTGAGTTCGCAG
Foxp3	TCCAGGTTGCTCAAAGTCTTCTTG	AGGCTGCTGTTACGGGAATAGG
Gata3	ACAGAAGGCAGGGAGTGTGTGAAC	TTTTATGGTAGAGTCCGCAGGC
Rorc	TCTACGCTATGAGGAAGGAAGGC	GACTATGGAGGAGAAACAGGTCCC
T-bet	ACCAACAACAAGGGGGCTTC	CTCTGGCTCTCCATCATTCACC

Figure S1

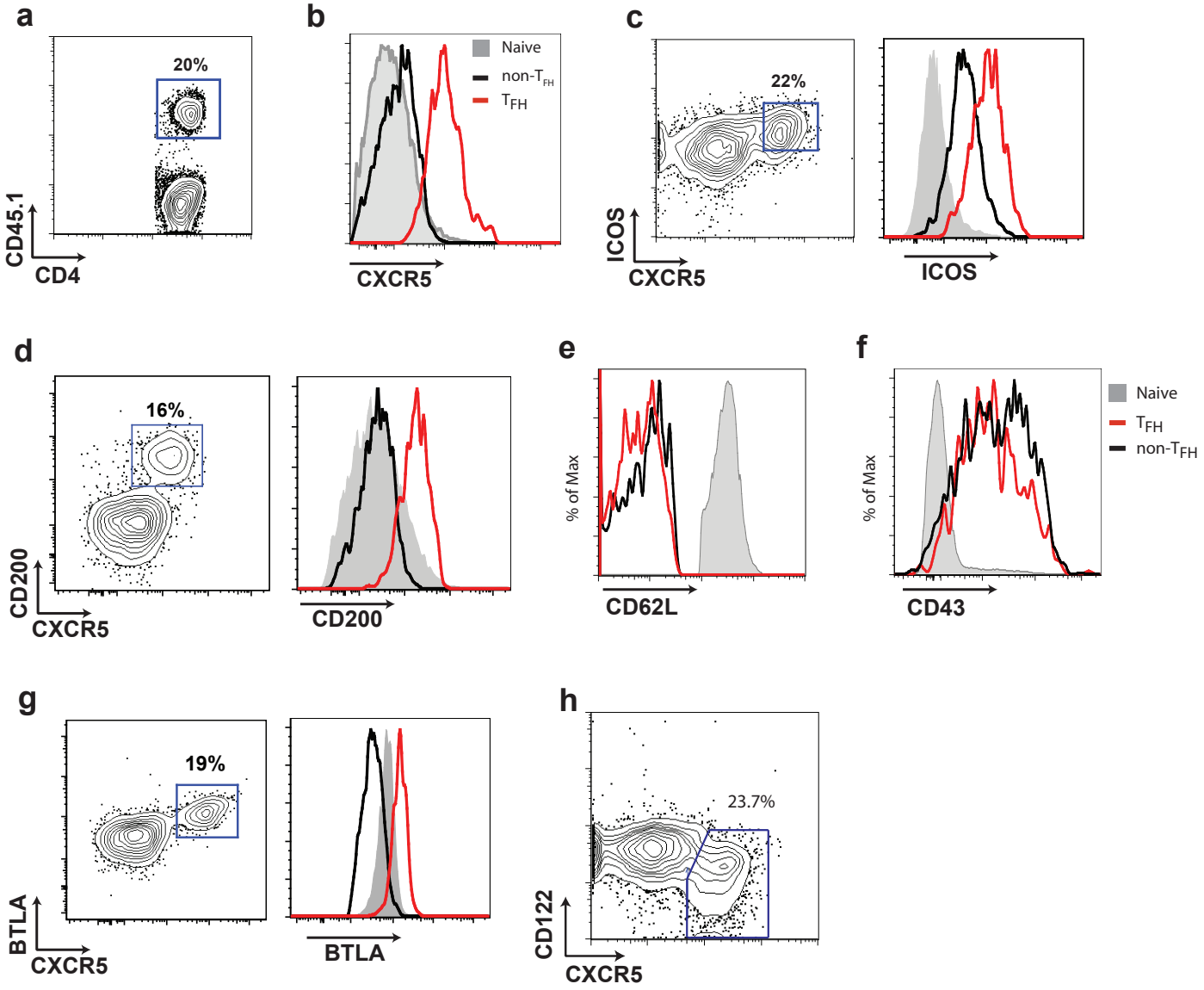

Figure S1. Phenotypic characterization of T_{FH}. Naïve SMtg CD4 T cells were transferred into B6 mice subsequently infected with LCMV. Splenocytes were analyzed 8 days after infection. **(A)** SMtg ($CD45.1^+$, boxed) and endogenous $CD4^+$ T cells (not boxed). $CD4^+B220^-$ gate is shown. Flow cytometry of **(B)** CXCR5, **(C)** ICOS, **(D)** CD200, **(E)** CD62L, **(F)** $CD43^{1B11}$, **(G)** BTLA, and **(H)** CD122 expression on SMtg $CD4^+$ T cells. FACS plots are gated on total SMtg $CD4^+$ T cells ($CD45.1^+CD4^+B220^-$). Histogram overlays are gated on naive CD4 T cells or SMtg CD4 T cells at day 8 after infection and depict $CXCR5^{high}$ T_{FH} (red), $CXCR5^{low}$ non-T_{FH} (black), and naive $CD4^+$ T cells (gray). In conjunction with the data shown in Figure 1, these results indicate that T_{FH} are not simply highly activated cells, as they have specifically downregulated SLAM and CD122, which are activation markers (*15, 16*), and have upregulated the inhibitory receptor BTLA (*17*), which is downregulated on most non-T_{FH} effector $CD4^+$ T cells. The T_{FH} also have equivalent expression to non-T_{FH} of activation markers CD62L and $CD43^{1B11}$. Data are representative of more than 10 independent experiments.

Figure S2

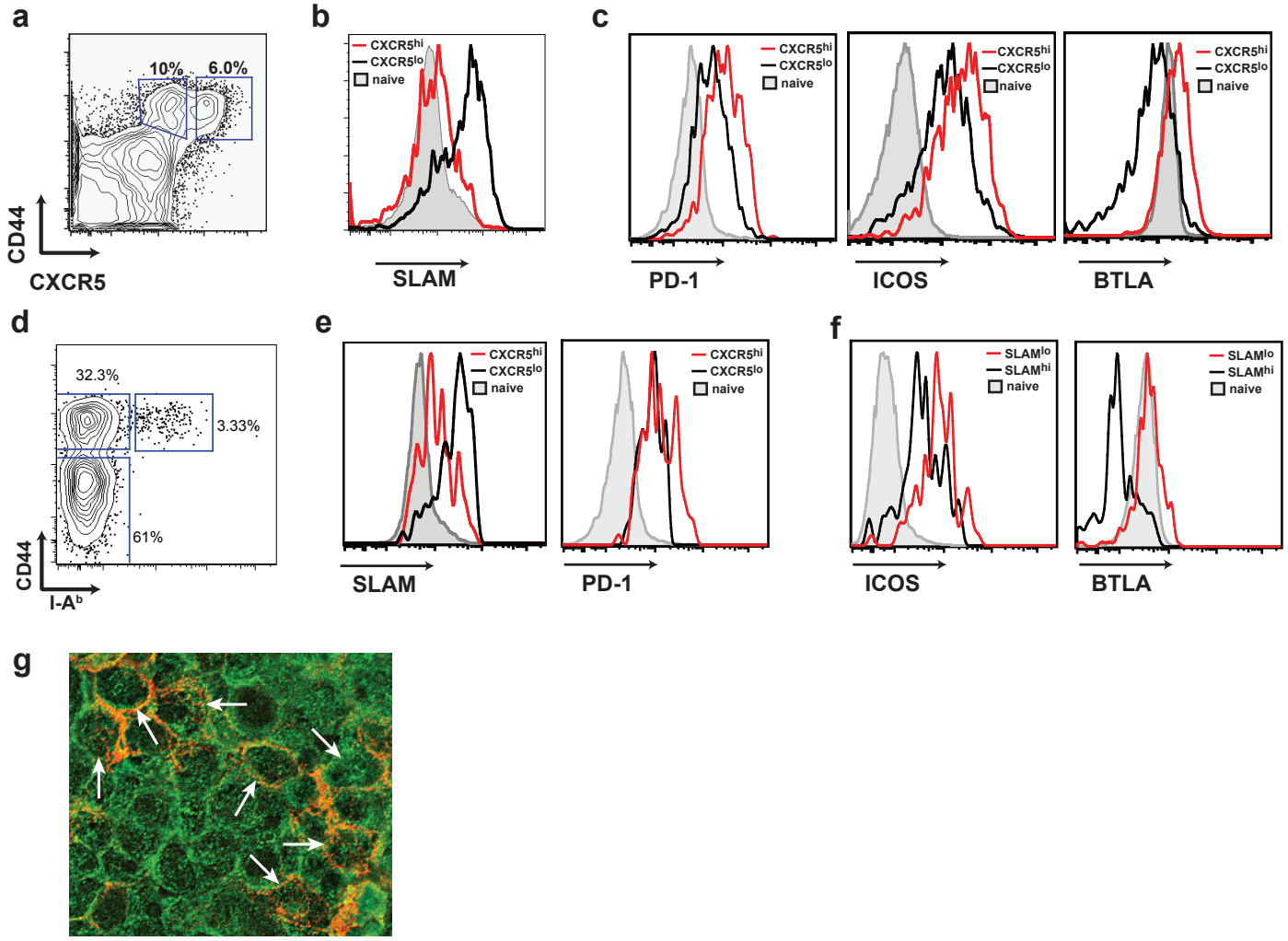

Figure S2. T_{FH} phenotypic characterization of polyclonal LCMV-specific $CD4^+$ T cells. T_{FH} phenotyping of polyclonal LCMV-specific $CD4^+$ T cell responses provided results comparable to that obtained with SMtg $CD4^+$ T cells. **(A)** Identification of endogenous $CXCR5^{high}$ (right gate) and $CXCR5^{low}$ populations (left gate) of $CD44^{high}$ (activated) $CD4^+$ T cells in LCMV-infected C57BL/6 mice. $CD4^+$ $B220^-$ gate is shown. While all $CD44^{high}$ $CD4^+$ T cells expressed more CXCR5 than $CD44^{low}$ (naive) $CD4^+$ T cells, consistent with the published literature that CXCR5 is an activation marker in mice (*18*), a $CXCR5^{high}$ $CD44^{high}$ population was clearly distinguishable among the $CD44^{high}$ cells. **(B)** SLAM expression in $CD44^{high}$ $CXCR5^{high}$ T_{FH} (red), $CD44^{high}$ $CXCR5^{low}$ non-T_{FH} (black), and naive $CD4^+$ T cells (gray). Only $CD44^{high}$ $CXCR5^{high}$ were $SLAM^{low}$ and defined as T_{FH}. **(C)** Further phenotypic analysis of endogenous T_{FH}. Expression of PD-1, ICOS, and BTLA are shown on T_{FH} ($SLAM^{low}$, red), non-T_{FH} ($SLAM^{high}$, black) and naive $CD4^+$ T cells (gray). All expression patterns were comparable to that observed with SMtg transgenic $CD4^+$ T cells. Data are representative of more than 10 independent experiments. **(D-F)** The T_{FH} phenotype was also confirmed in polyclonal LCMV-specific $CD4^+$ T cells using gp66-77 $I\text{-}A^b$ MHC-II tetramer staining to analyze C57BL/6 splenocytes 10 days after infection with LCMV. **(D)** Identification of MHC-II gp66-$tetramer^+$ $CD4^+$ T cells (top right gate). $CD4^+$ $B220^-$ gate is shown. **(E)** Phenotypic analysis of $tetramer^+$ T_{FH}, on the basis of CXCR5 staining. SLAM and PD-1 staining are shown. **(F)** Phenotypic analysis of $tetramer^+$ T_{FH}, on the basis of SLAM staining. ICOS and BTLA staining are shown. Data are representative of 2 or more independent experiments. All expression patterns were comparable to that observed with SMtg transgenic $CD4^+$ T cells or polyclonal $CD44^{hi}$ $CD4^+$ T cells at day 8 post-infection. **(G)** Immunofluorescence histology of spleen sections, 15 days after LCMV infection. Co-staining of a germinal center (PNA stain not shown) with anti-Bcl6 (green) and anti-CD4 (orange). All non-CD4 T cells are germinal center B cells, and all germinal center B cells are positive for intracellular BCL6. The majority of $CD4^+$ T cells (indicated by white arrows) are also positive for intracellular BCL6.

Figure S3

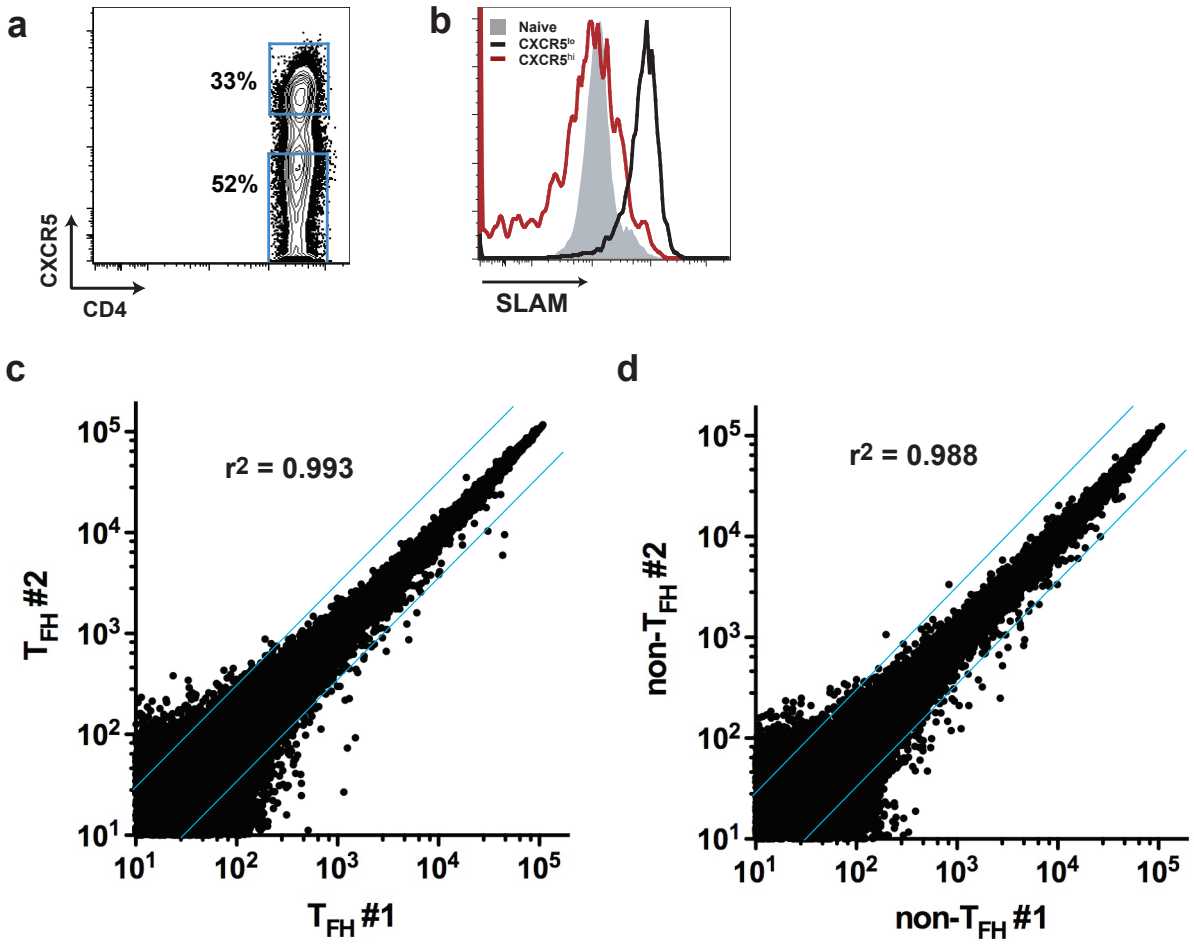

Figure S3. Gene expression microarray analysis of *in vivo* antigen-specific T_{FH}. SMtg $CD4^+$ T cells were transferred into C57BL/6 mice subsequently infected with LCMV. **(A)** SMtg T_{FH} (top gate) and non-T_{FH} (bottom gate) were then sorted on the basis of CXCR5 expression. $CD4^+CD45.1^+TCR\beta^+CD19^-7AAD^-$ cell gate is shown. Biological replicate samples were collected for each condition (sample #1 and sample #2). **(B)** SLAM expression was confirmed on $CXCR5^+$ and $CXCR5^-$ SMtg $CD4^+$ T cells using an aliquot of cells in an independent stain prior to sorting the cells used in panel A. **(C)** Gene expression microarray analysis (as per Fig. 1E). Scatter plot of T_{FH} sample 1 vs T_{FH} sample 2 microarray data. Each gene probe is shown as an individual point. Replicate samples were highly correlated, $r^2 = 0.993$. **(D)** Non-T_{FH} sample 1 vs. non-T_{FH} sample 2 microarray data. Replicate samples were highly correlated, $r^2 = 0.988$.

Figure S4

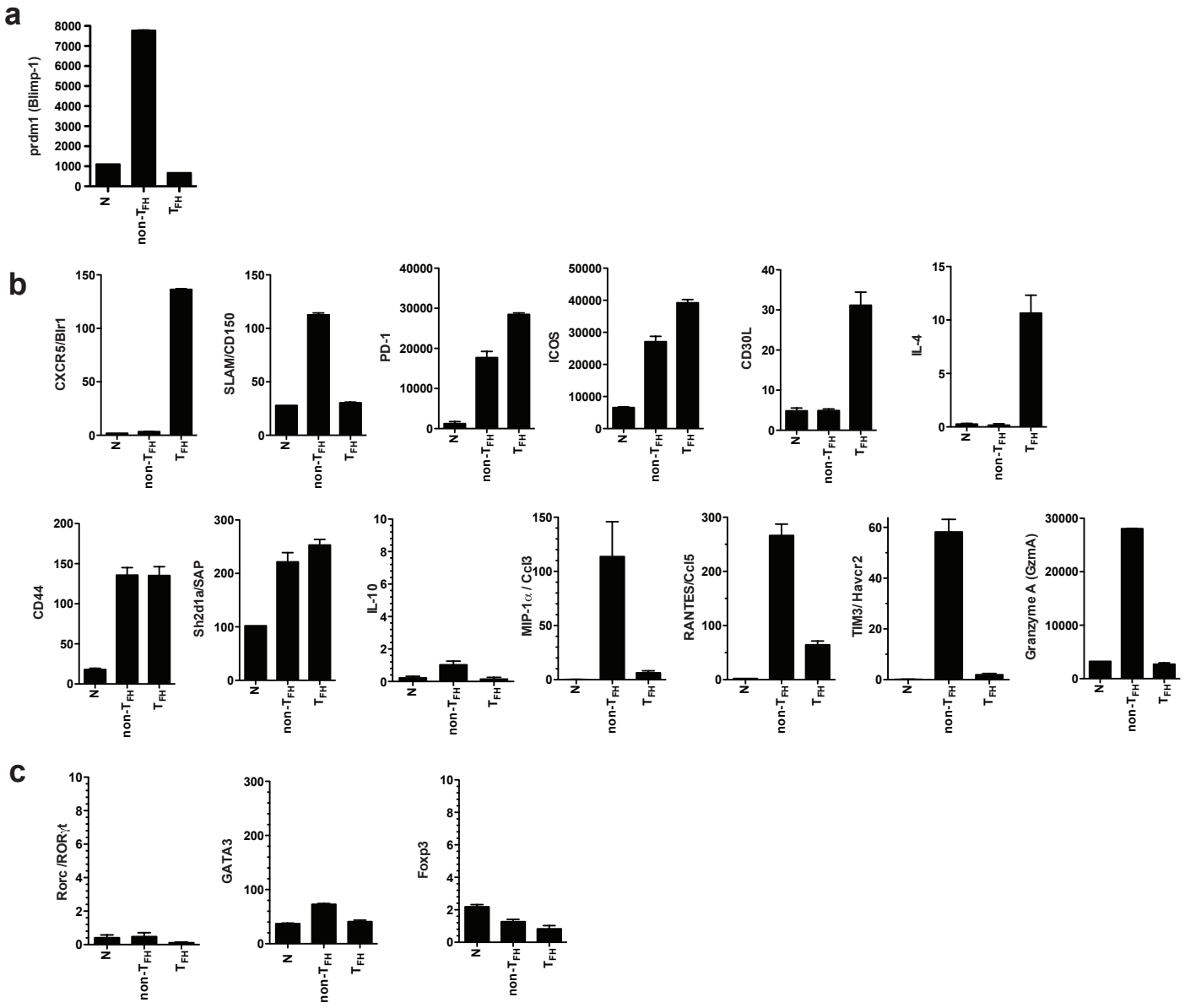

Figure S4. Gene expression microarray analysis of *in vivo* antigen-specific T_{FH}. (A-C) Gene expression microarray data of selected genes in naive $CD4^+$ T cells (N), SMtg non-T_{FH}, and SMtg T_{FH} from the cells described in Figure S3.

Figure S5

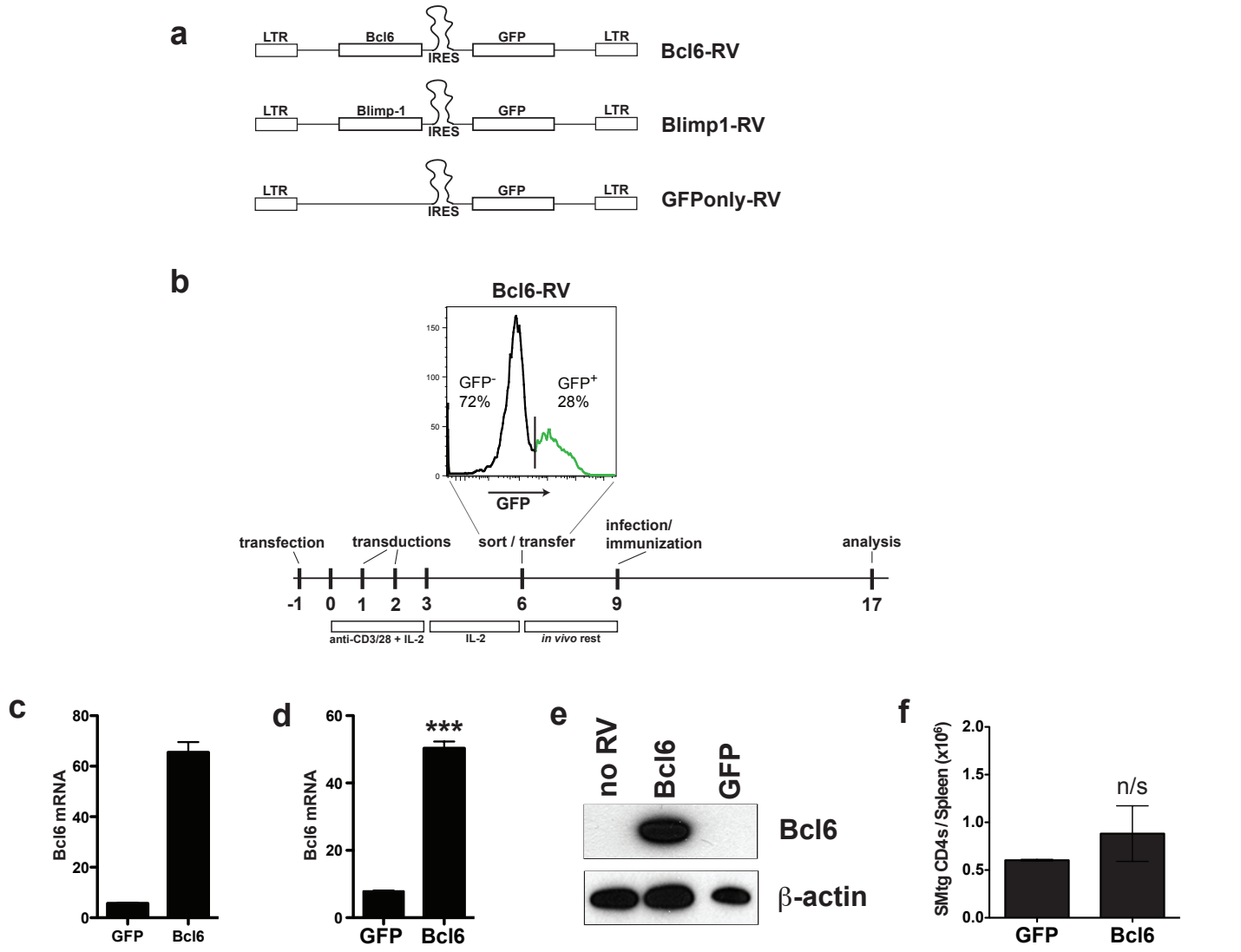

Figure S5. Retroviral expression vectors and transduction schema. (A) Bcl6 (Bcl6-RV), Blimp1 (Blimp1-RV) and control (GFP-RV, expressing only GFP) retroviral constructs. **(B)** A brief retroviral transduction and adoptive transfer schematic, with Bcl6-RV$^+$ FACS at the time of sort. Details provided in Methods. **(C-D)** Bcl6 qPCR using Bcl6-RV$^+$ (transduced) SMtg CD4$^+$ T cells **(C)** *in vitro* and **(D)** after transfer into C57BL/6 mice subsequently infected with LCMV. Day 8 post-infection, as per Figure 1. GFP-RV$^+$ CD4$^+$ T cells shown for comparison. **(E)** Bcl6 immunoblot with lysates from transfected and non-transfected Plat-E cells. **(F)** Expansion of Bcl6-RV$^+$ and GFP-RV$^+$ SMtg cells *in vivo*, day 8 after LCMV infection, as per Figure 2, A-E. Graph depicts total Bcl6-RV$^+$ or GFP-RV$^+$ SMtg CD4$^+$ T cells per spleen. No significant difference in expansion was observed between the groups (NS, not significant. $P > 0.05$).

Figure S6

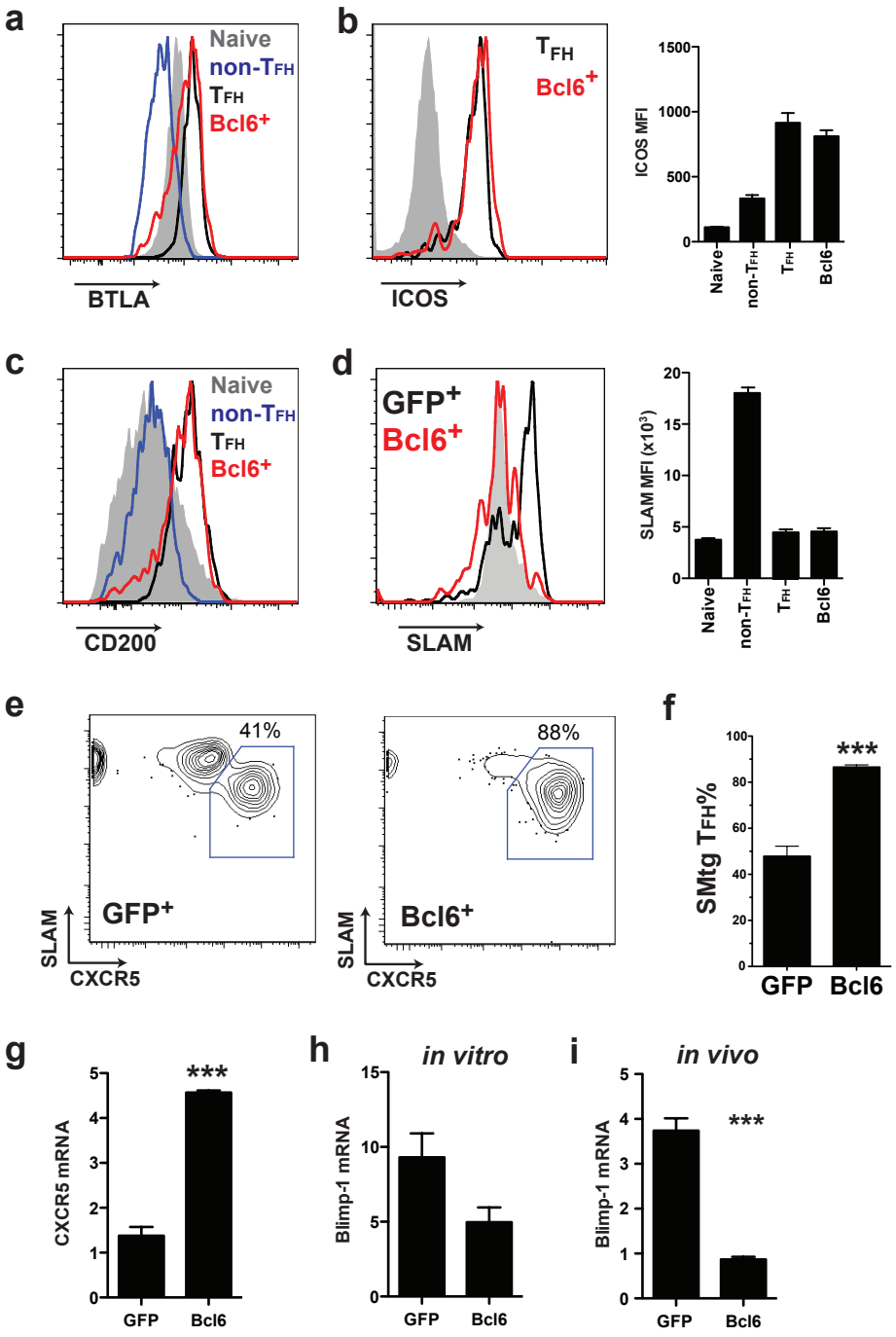

Figure S6. Phenotypic analysis of Bcl6-RV$^+$ CD4$^+$ T cells *in vivo*. In conjunction with the data shown in Figure 2, these data indicated Bcl6 expression drives full T_{FH} differentiation *in vivo*. Histogram overlays and MFI bar graphs depicting expression of **(A)** BTLA, **(B)** ICOS, **(C)** CD200, and **(D)** SLAM in naïve CD4$^+$ T cells (gray), GFP-RV$^+$ SMtg non-T_{FH} (blue), GFP-RV$^+$ SMtg T_{FH} (black), and Bcl6-RV$^+$ SMtg (red). Data shown are from the same experiments as shown in Figure 2. **(E-F)** Differentiation of GFP-RV$^+$ SMtg ("GFP+") or Bcl6-RV$^+$ SMtg ("Bcl6+") within independent hosts. All mice were infected with LCMV after the cell transfers. Experiments were performed comparably to those described in Figure 2, except mice received either GFP-RV$^+$ or Bcl6-RV$^+$ cells. n = 4/group. Data are representative of 6 independent experiments. **(E)** T_{FH} (SLAM^{low} CXCR5^{high}, boxed) and non-T_{FH} (SLAM^{high} CXCR5^{low}) differentiation of GFP-RV$^+$ SMtg ("GFP+") and Bcl6-RV$^+$ SMtg ("Bcl6+"). **(F)** Quantitation of SMtg T_{FH} differentiation. ***, P = 0.0002. **(G)** CXCR5 qPCR in Bcl6-RV$^+$ and GFP-RV$^+$ B6 CD4$^+$ T cells cultured *in vitro*. ***, P < 0.0001. **(H-I)** Blimp-1 qPCR in Bcl6-RV$^+$ and GFP-RV$^+$ B6 CD4$^+$ T cells **(H)** cultured *in vitro* and **(I)** after transfer into C57BL/6 mice subsequently infected with LCMV.

Figure S7

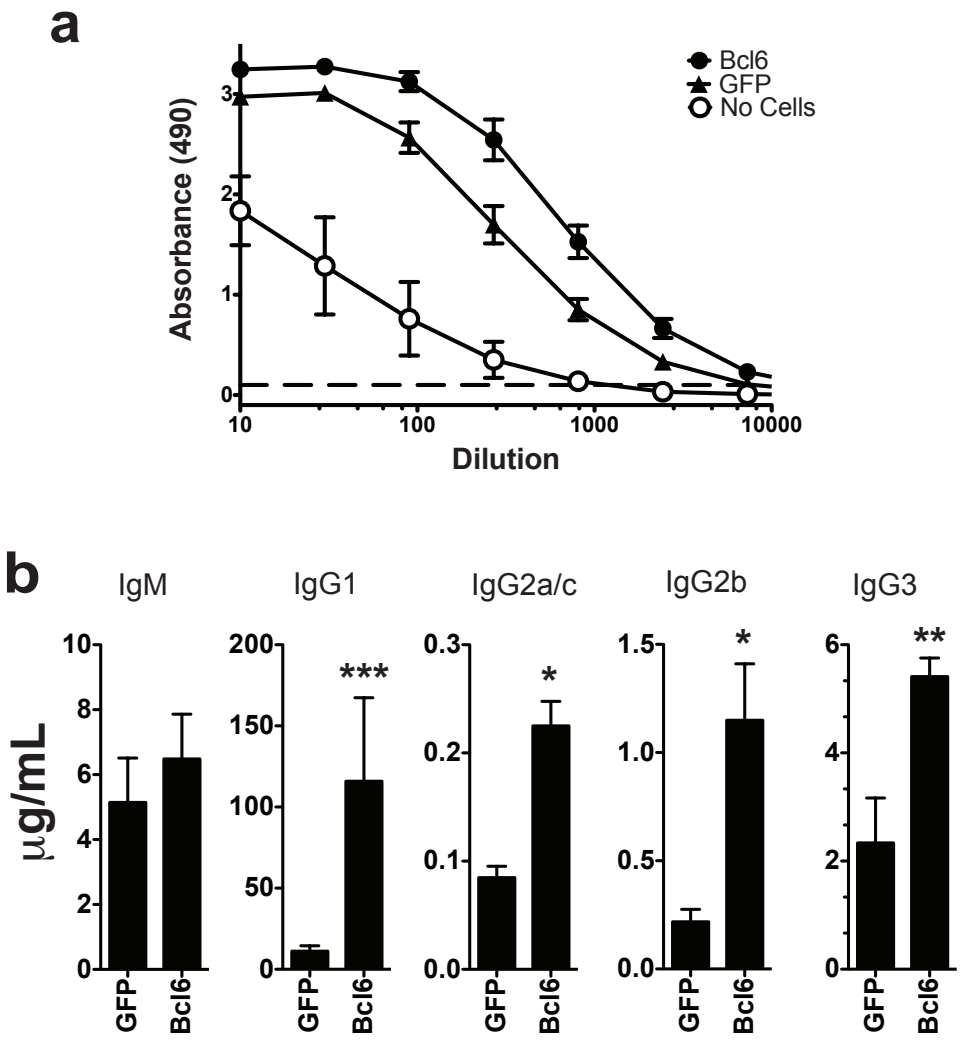

Figure S7. Constitutive Bcl6 expression in CD4$^+$ T cells drives enhanced antibody responses in vivo. Day 8 **(A)** IgGγ and **(B)** isotype-specific anti-NP-Ova ELISA data for samples from the Bcl6-RV$^+$ SMtg vs. GFPonly-RV$^+$ SMtg study described in Figure 3B to C. IgG1, ***, P = 0.0009. IgG2a/c, *, P = 0.019. IgG2b, *, P = 0.039. IgG3, **, P = 0.0065. NP-Ova specific IgM levels were not affected by constitutive expression of Bcl6, suggesting that IgM production is not T_{FH} dependent.

Figure S8

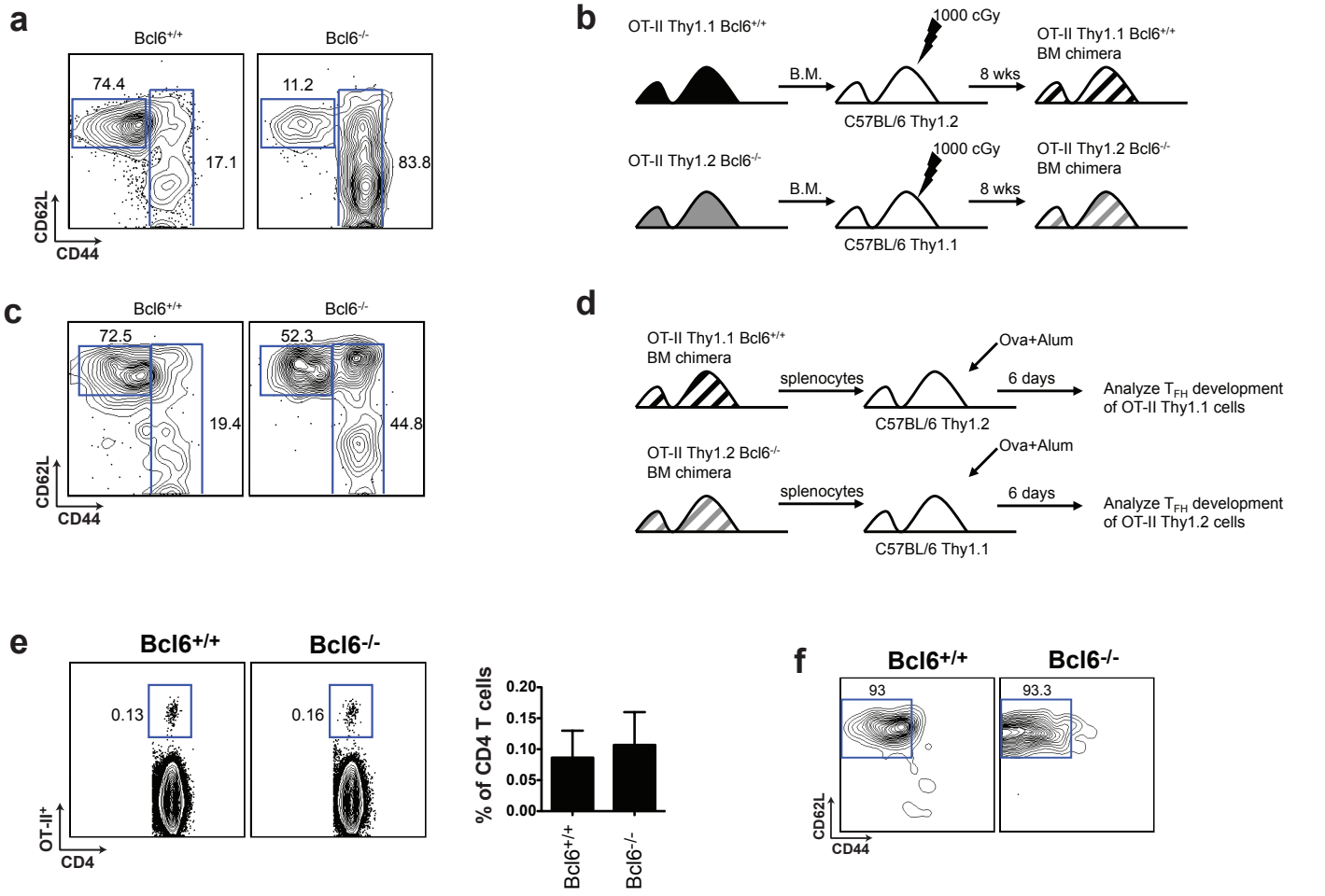

Figure S8. Generation and characterization of *Bcl6*$^{-/-}$ OT-II CD4^{+} T cells. **(A)** Activation state of *Bcl6*$^{+/+}$ and *Bcl6*$^{-/-}$ OT-II cells. Splenic CD4^{+} T cells from 3-4 week old mice are shown. **(B)** Diagram of bone marrow chimera generation. T-depleted bone marrow from OT-II *Bcl6*$^{+/+}$ and *Bcl6*$^{-/-}$ mice was transferred into irradiated, congenically mismatched C57BL/6 mice. **(C)** Activation state of *Bcl6*$^{+/+}$ and *Bcl6*$^{-/-}$ OT-II cells isolated from bone marrow chimeras after 8 weeks. **(D)** Splenocytes were transferred from bone marrow chimeras into congenically mismatched recipient mice for experiments. **(E-F)** *Bcl6*$^{-/-}$ OT-II CD4^{+} T cells obtained from chimeric mice did not exhibit lymphoproliferation or spontaneous activation after adoptive transfer. Cell frequencies and numbers **(E)** and activation state **(F)** of OT-II *Bcl6*$^{+/+}$ and *Bcl6*$^{-/-}$ splenic CD4^{+} T cells as described in Figure 3 but in animals that were not immunized.

Figure S9

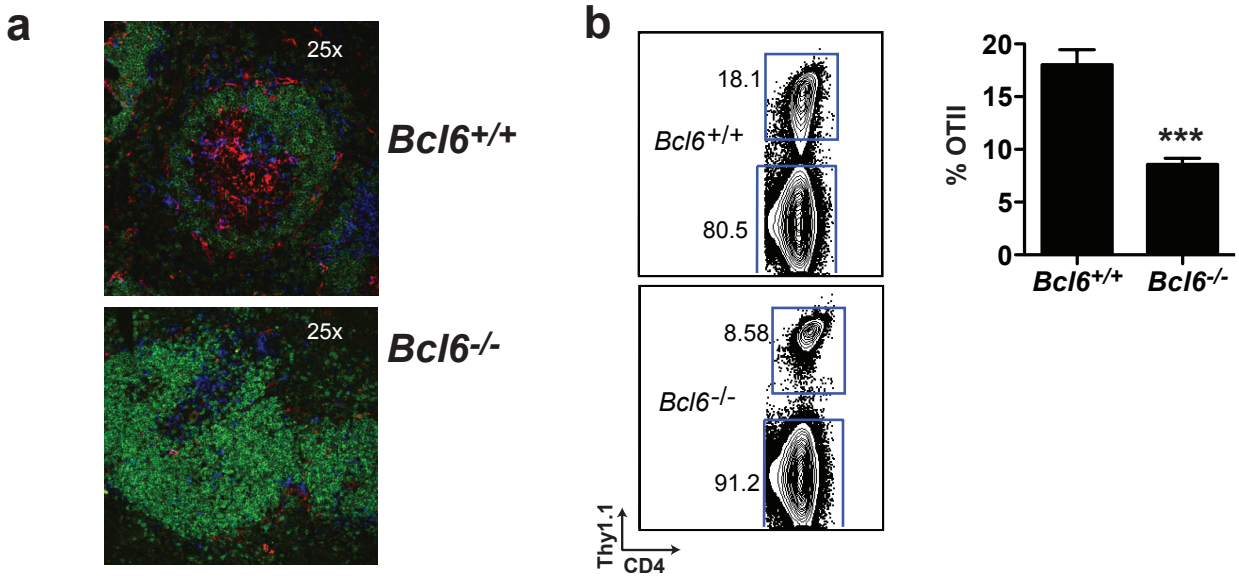

Figure S9. Germinal center formation is dependent on Bcl6 expression by CD4$^+$ T cells. (A) High power images of germinal center histology, from the experiment described in Figure 3E-G: *Bcl6*$^{+/+}$ or *Bcl6*$^{-/-}$ OT-II CD4$^+$ T cells were co-transferred with B1-8 B cells into *Icos*$^{-/-}$ mice subsequently immunized with NP-Ova in alum. Spleen sections were stained with IgD (green), PNA (red), and CD4 (blue). **(B)** Expansion of *Bcl6*$^{+/+}$ and *Bcl6*$^{-/-}$ OT-II CD4$^+$ T cells as described in Figure 3D. CD4$^+$ splenocytes are shown.

Figure S10

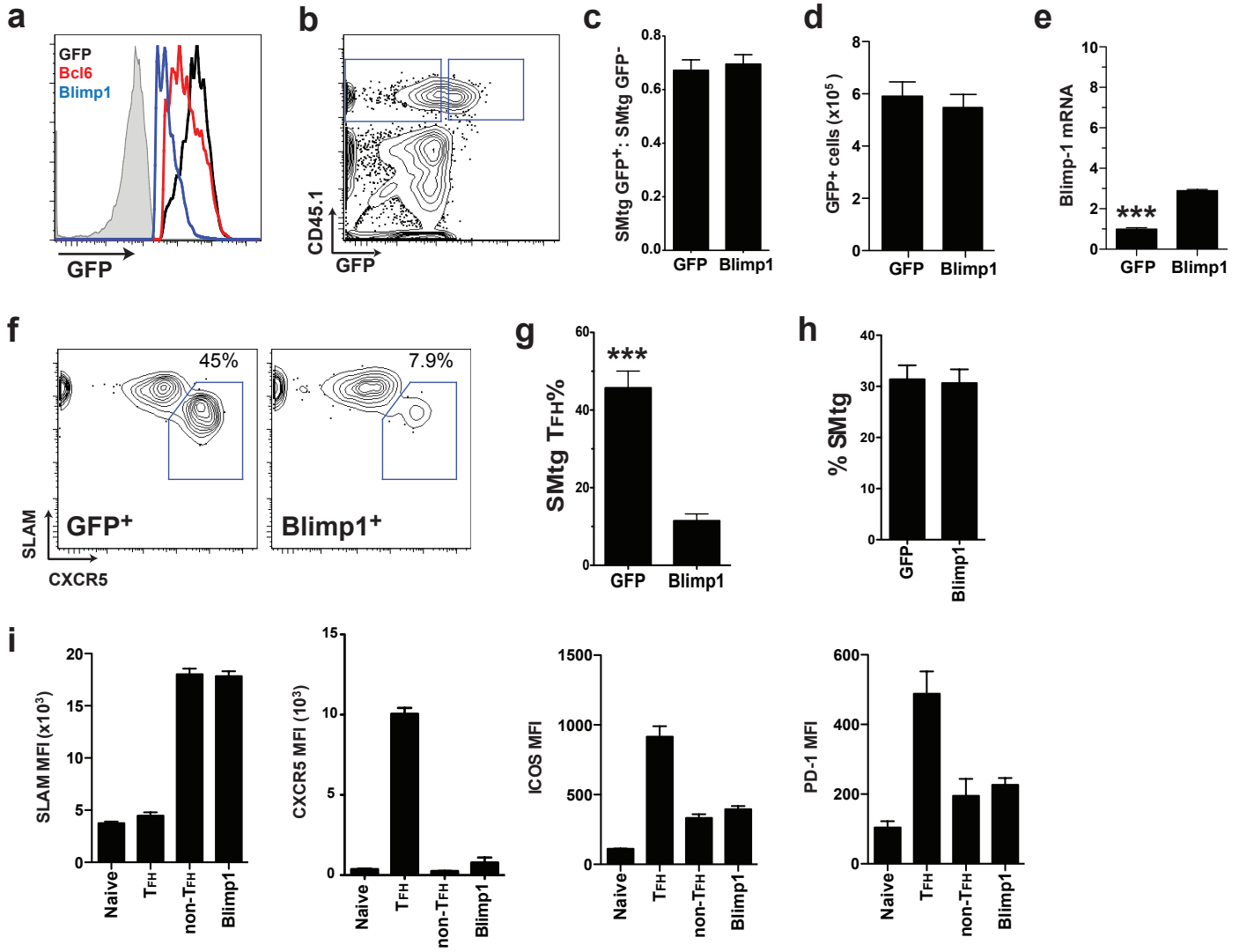

Figure S10. Constitutive Blimp-1 expression selectively blocks T_{FH} differentiation of CD4$^+$ T cells *in vivo*. (A) Histogram overlay of GFP expression in untransduced (gray), GFP-RV$^+$ (black), Bcl6-RV$^+$ (red), and Blimp1-RV$^+$ (blue) SMtg CD4$^+$ T cells *in vitro*, during cell sorting, prior to adoptive transfer. **(B-I)** All data shown is from experiments at day 8 after LCMV infection. **(B)** Cell gating for Figure 4B. CD4$^+$B220$^-$ gate is shown. Transduced (right gate, GFP$^+$ CD45.1$^+$ SMtg cells. "Blimp1") and untransduced (left gate, GFP$^-$ CD45.1$^+$ SMtg cells. "Control") cells. **(C-D)** Quantitation of GFP-RV$^+$ and Blimp1-RV$^+$ SMtg cells *in vivo*, for the experiment shown in Figure 4B-C. **(C)** Ratio of transduced (Blimp1 or GFP) SMtg to GFP$^-$ (untransduced) SMtg. **(D)** Number of GFP-RV$^+$ or Blimp1-RV$^+$ SMtg CD4$^+$ T cells per spleen. n = 4/group. Data are representative of 2 independent experiments. **(E)** qPCR of Blimp-1 mRNA in total GFP-RV$^+$ SMtg (non-T_{FH} and T_{FH}) and total Blimp1-RV$^+$ SMtg from LCMV infected mice, normalized to the β-actin mRNA level (x 10^{-4}). ***, $P < 0.0001$. **(F-I)** Differentiation of GFP-RV$^+$ SMtg ("GFP+") or Blimp1-RV$^+$ SMtg ("Blimp1+") within independent hosts subsequently infected with LCMV. Experiments were performed comparably to those described in Figure 4, except mice only received either GFP-RV$^+$ or Blimp1-RV$^+$ cells. n = 4/group. Data are representative of more than 4 independent experiments. **(F)** Flow cytometry of T_{FH} (SLAM^{low} CXCR5^{high}, boxed) and non-T_{FH} (SLAM^{high} CXCR5^{low}) differentiation of GFP-RV$^+$ SMtg or Blimp1-RV$^+$ SMtg. **(G)** Quantitation of SMtg T_{FH} differentiation. ***, $P = 0.0002$. **(H)** SMtg expansion, as a percentage of CD4$^+$ T cells in the spleen. No difference was observed. **(I)** Expression levels (MFIs) of SLAM, ICOS, and PD-1 on naïve CD4$^+$ T cells, GFP-RV$^+$ SMtg non-T_{FH} ("non-T_{FH}"), GFP-RV$^+$ SMtg T_{FH} ("T_{FH}"), and Blimp1-RV$^+$ SMtg ("Blimp1"). No significant differences in expression were observed between GFP-RV$^+$ SMtg non-T_{FH} and total Blimp1-RV$^+$ SMtg for any of these proteins.

Figure S11

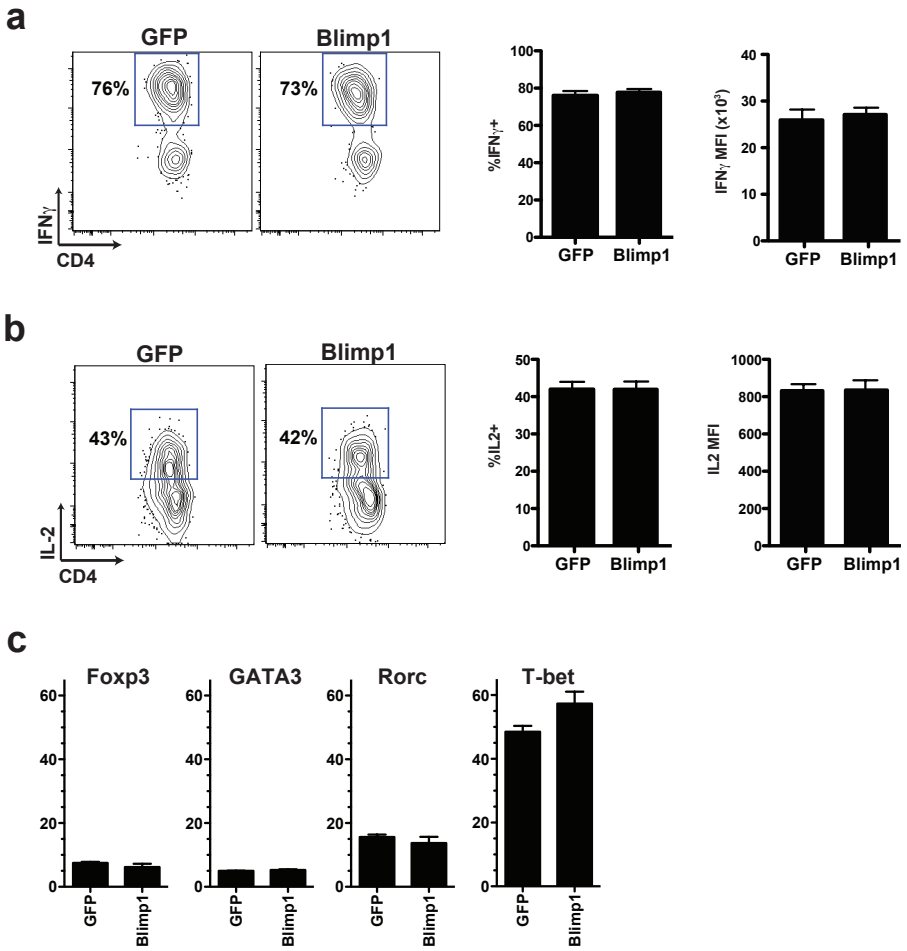

Figure S11. Cytokine production by Blimp1-RV$^+$ SMtg CD4$^+$ T cells. Blimp1-RV$^+$ and GFP-RV$^+$ SMtg cells were transferred into C57BL/6 mice subsequently infected with LCMV. Cells were analyzed at day 8 after infection. **(A)** Intracellular staining for IFNγ in GFP-RV$^+$ CXCR5^{low} non-T_{FH} and Blimp1-RV$^+$ CXCR5^{low} non-T_{FH}. Bar graphs show quantification of % IFNγ$^+$ non-T_{FH} SMtg, and IFNγ MFI. No differences were observed. **(B)** Intracellular staining for IL-2 in GFP-RV$^+$ CXCR5^{low} non-T_{FH} and Blimp1-RV$^+$ CXCR5^{low} non-T_{FH}. Bar graphs show quantification of % IL-2$^+$, and IL-2 MFI. No differences were observed. **(C)** Foxp3, GATA3, Rorc and T-bet qPCR in GFP-RV$^+$ and Blimp1-RV$^+$ non-T_{FH}, normalized to the β-actin mRNA level (x 10^{-4}). No differences were observed.

Figure S12

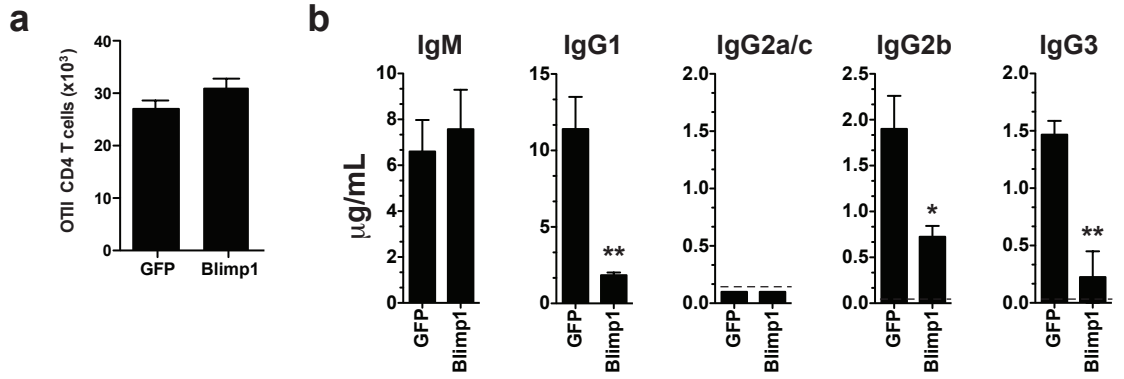

Figure S12. Constitutive Blimp-1 expression in CD4$^+$ T cells prevents antigen-specific IgG responses of all isotypes. Blimp1-RV$^+$ and GFP-RV$^+$ OT-II cells were transferred into *SAP*$^{-/-}$ mice subsequently immunized with NP-Ova in alum. Experiment is the same as Figure 4E to F. **(A)** Number of transduced OT-II cells per spleen. **(B)** Day 10 isotype-specific anti-NP-Ova antibody titers. IgM, not significant. IgG1, **, P = 0.0029. IgG2a/c, not detected. IgG2b, *, P = 0.017. IgG3, **, P = 0.0073. All IgG isotypes were reduced in Blimp1-RV$^+$ recipient mice. IgM levels were again unaffected, suggesting that IgM production is not T_{FH} dependent.

Figure S13

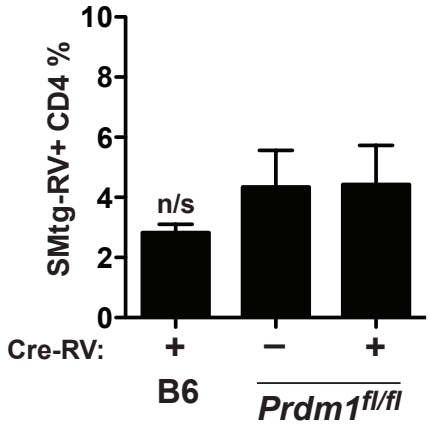

Figure S13. RV-transduced *Prdm1*$^{fl/fl}$ CD4^{+} T cells proliferate normally. C57BL/6 and *Prdm1*$^{fl/fl}$ CD4^{+} T cells were transduced and transferred into SAP-deficient CD45.1^{+} mice subsequently infected with LCMV, as described in Figure 4G. **(A)** Expansion of the transduced CD4^{+} T cells after LCMV infection, as a percentage of total CD4^{+} T cells in the spleen. No significant differences were observed between the groups (NS, not significant. $P > 0.05$).

Figure S14

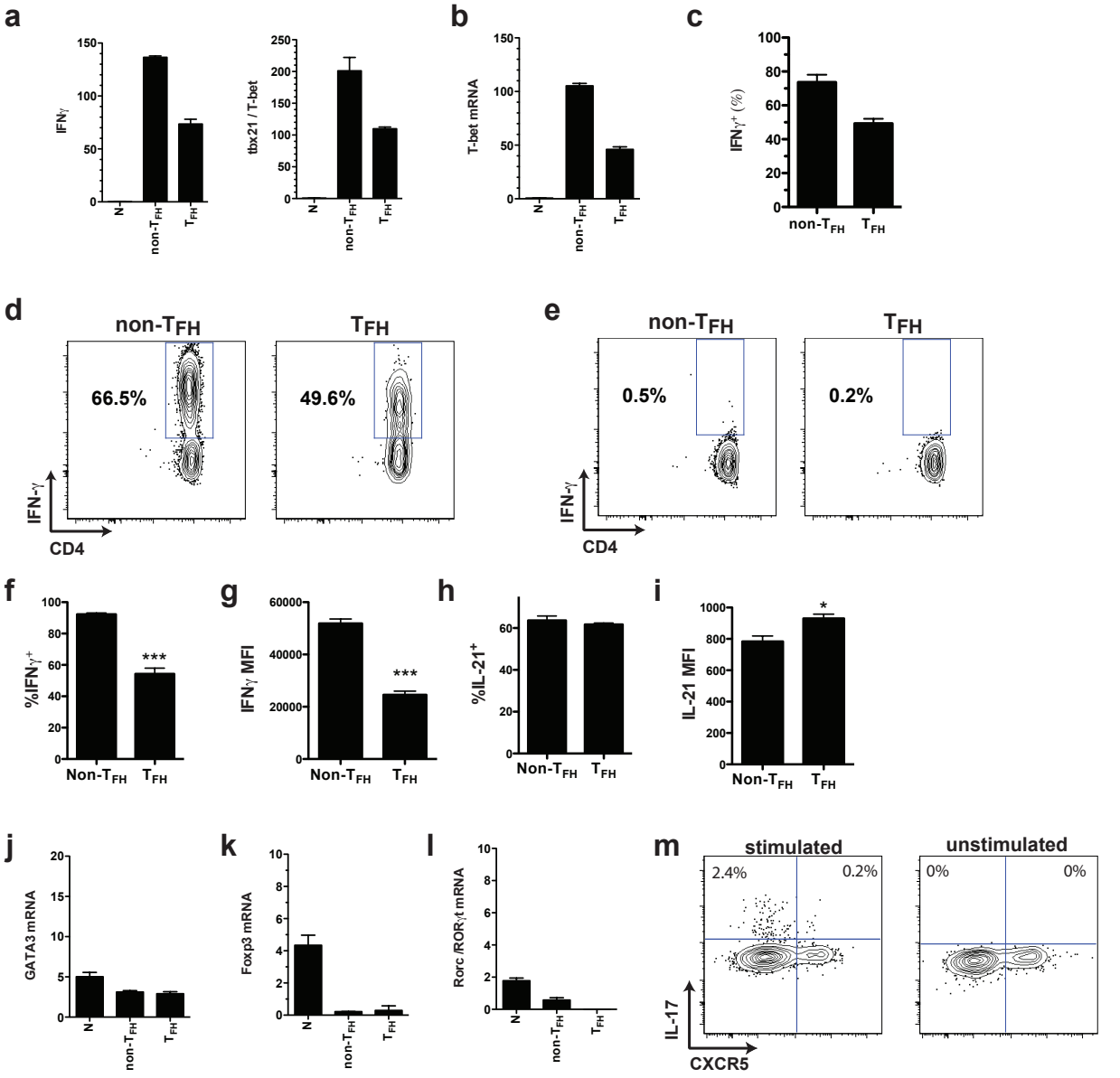

Figure S14. Analysis of cytokines and T_H1, T_H2, T_{reg}, and T_H17 related genes in T_{FH}. (A) Microarray signals of T_H1 genes IFNγ and T-bet (*tbx21*) are reduced in T_{FH} vs. non-T_{FH} *in vivo*. N = Naive SMtg $CD4^+$ T cells. **(B)** qPCR of T-bet from the same RNA, normalized to the β-actin mRNA level (x 10^{-4}). **(C-E)** The predominant $CD4^+$ T cell response to LCMV is T_H1 (*19, 20*). IFNγ expression in T_{FH} and non-T_{FH} after *ex vivo* stimulation with antigen presenting cells plus peptide (LCMV gp66-77). n = 4/group. Data are representative of 3 independent experiments. **(C)** Quantitation and **(D)** representative FACS plots of IFNγ intracellular cytokine staining in **(D)** peptide stimulated and **(E)** unstimulated SMtg $CD4^+$ T cells. **(F-I)** Cytokine production by SMtg $CD4^+$ T cells after *ex vivo* stimulation with PMA and ionomycin. n = 4/group. Data are representitive of 3 independent experiments. **(F)** % $IFN\gamma^+$ T_{FH} and non-T_{FH}. The percentage of $IFN\gamma^+$ cells was somewhat reduced in T_{FH}. **(G)** IFNγ MFI of $IFN\gamma^+$ cells in (F). The expression level (MFI) of IFNγ was somewhat reduced in T_{FH}, among $IFN\gamma^+$ cells. **(H)** % $IL\text{-}21^+$ in T_{FH} and non-T_{FH}. **(I)** IL-21 MFI of $IL\text{-}21^+$ cells in (H). **(J-L)** qPCR for the $CD4^+$ T cell transcription factors **(J)** GATA3 (normalized to the β-actin mRNA level (x 10^{-4})), **(K)** Foxp3 (normalized to the β-actin mRNA level (x 10^{-5})), **(L)** RORγt (normalized to the β-actin mRNA level (x 10^{-5})). **(M)** IL-17 intracellular cytokine staining in SMtg T_{FH} and non-T_{FH} 8 days after LCMV infection. No significant production was observed.